Atomistic structure of calcium silicate intergranular films between prism and basal planes in silicon nitride: A molecular dynamics study

Xiaotao Su and Stephen H. Garofalini
Department of Ceramics and Materials Engineering, Rutgers University, Piscataway, New Jersey 08854

(Received 10 September 2003; accepted 31 October 2003)

Molecular dynamics simulations of approximately 15 Å thick intergranular films (IGFs) containing SiO_2 and CaO in contact with two surface terminations of the prism $(10\bar{1}0)$ and basal planes (0001) of Si_3N_4 were performed using a multibody interatomic potential. Samples with the same composition (1.5 mol% CaO) and number of atoms but different crystal planes (i.e., the prism and basal planes of Si_3N_4) were studied. In both the prism and basal cases, the IGF in the final configuration is well-ordered in the interface region. A small number of N ions from the crystal moved into the IGF near the interface, and O ions moved into the N sites in the crystal, indicating the formation of a Si–O–N interface. In addition, Ca ions do not segregate to the IGF–crystal interface. The bonding characteristics of the O ions at the interface with neighbor Si ions are different in the prism and basal cases. Such difference may be explained by the difference in the two crystal Si_3N_4 surfaces. The Si–O bond length of the IGF has a range from 1.62 Å to 1.64 Å, consistent with recent experimental findings.

I. INTRODUCTION

Silicon nitride (Si_3N_4)-based materials are considered promising structural ceramics for high-temperature applications. In the intergranular regions between Si_3N_4 grains, there are typically secondary amorphous phases, which form glass pockets at triple-grain junctions and thin amorphous intergranular films (IGFs) at grain boundaries. Such intergranular films were observed in the late 1970s.[1–3] The properties of the intergranular phases determine the overall diffusion-related behavior of the material, such as creep, oxidation, and high-temperature strength of Si_3N_4.[4–6] Kleebe and coworkers showed that the thickness of the intergranular films strongly depends on film chemistry and is constant within ±1 Å.[7–9] Clarke et al.[10,11] developed a model in which equilibrium film thickness is determined by the balance between the attractive van der Waals force acting across the IGF and a repulsive term due to the steric force and the electrical double-layer force in the intergranular films. Tanaka and coworkers[12] characterized both the intergranular silicate film thickness and its local composition in a series of high-purity Si_3N_4 ceramics doped with 0–450 at. ppm Ca. They found that the thickness of the intergranular films at two-grain junctions depends sensitively on Ca content. In undoped material, the thickness was 10 ± 1 Å. When Ca content increased, the thickness decreased in dilute region (less than 80 ppm Ca), but then increased. Assuming that all Ca and O are localized in the intergranular phase, the calcium concentration at the two-grain junctions in the 80-ppm-doped material was found to be 1.5 ± 0.3 mol% CaO/(CaO + SiO_2).[12] In this paper, we focus on IGFs with calcium concentration of 1.5 mol%.

II. COMPUTATIONAL PROCEDURE

Molecular dynamics simulations have been performed to simulate the interfaces. To describe the interactions between ions, we have used a multibody interatomic potential, which consists of both 2- and 3-body terms

$$V = \sum_{i \neq j} V_{ij}^{\mathrm{BMH}} + \sum_{i \neq j \neq k} V_{ijk}^{3\text{–body}} \quad . \tag{1}$$

where V_{ij}^{BMH} is the modified Born–Mayer–Huggins (BMH) pair potential, and $V_{jik}^{3\text{–body}}$ is the 3-body potential term.

The modified BMH pair potential is given by

$$V_{ij}^{\mathrm{BMH}} = A_{ij} \exp\left(\frac{-r_{ij}}{\rho_{ij}}\right) + \frac{z_i z_i e^2}{r_{ij}} \operatorname{erfc}\left(\frac{r_{ij}}{\beta_{ij}}\right) \quad . \tag{2}$$

where r_{ij} is the separation distance between ions i and j, e is the elementary charge, z_i and z_j are taken as full charge of the ions, and erfc is the complementary error function. The value of the parameters A_{ij}, β_{ij} and ρ_{ij} for

each pair type are listed in Table I. Atomic charges for silicon, oxygen, nitrogen and calcium ions are +4, −2, −3 and +2, respectively.

The 3-body potential acts as a penalty function, which increases the energy when the bond angle between covalently bonded species deviates from the preferred value. This 3-body potential is applied to all first neighbor triplets of the type (Si/Ca–O–Si/Ca, Si–N–Si, and O/N–Si–O/N), and is defined as follows:

$$V_{jik}^{3\text{–body}} = \lambda_{jik} \exp\left(\frac{\gamma_{ij}}{r_{ij} - r_{ij}^0} + \frac{\gamma_{ik}}{r_{ik} - r_{ik}^0}\right)\Omega_{jik} \quad , \quad (3)$$

when $r_{ij} < r_{ij}^0$ and $r_{ik} < r_{ik}^0$. Otherwise, $V_{jik}^{3\text{–body}} = 0$.

The angular part, Ω_{jik}, is defined as

$$\Omega_{jik} = (\cos\,\theta_{jik} + \cos\,\theta_{jik}^0)^2 \quad . \quad (4)$$

where θ_{jik} is the angle formed by the ions j, i, and k, with the ion i at the vertex. As the bonding of Ca is predominantly ionic, no 3-body potential is applied to calcium as the central ion. The parameters used for all 3-body potentials are listed in Table II. This multibody potential has previously been used in simulations of oxide glasses and glass surfaces[13–19] and interfaces.[20–23]

In the current work, we created an interface system by forming a glassy intergranular film from a random stoichiometric mixture of 3740 atoms (1234 Si, 2487 O, and 19 Ca) in contact with two prism crystal surfaces $(10\bar{1}0)$ of β-Si_3N_4. Similarly, we set up another interface system in which the same glassy intergranular film as above is in contact with two basal crystal surfaces (0001) of β-Si_3N_4. Periodic boundary conditions were applied in the x, y, and z directions. The simulated Si_3N_4 crystal consisted of 14112 atoms, with dimensions 53.25 Å × 52.40 Å × 52.70 Å for the prism case and 53.25 Å × 52.70 Å × 52.40 Å for the basal case. The calcium concentration in the IGF is 1.5 mol% CaO/(CaO + SiO_2), and the initial thickness of the film was approximately 20 Å.

The heat and quench process is summarized in Table III. The atoms in the Si_3N_4 crystals were immobilized from 10,000 K to 4000 K and were released and allowed to relax in the presence of the IGF from 3000 K to 300 K. The random mixtures of atoms were initially heated to 10,000 K to form a low-viscosity liquid in contact with the Si_3N_4 crystal surface, under conditions of constant number, volume, and energy. These systems were subsequently quenched to 8000 K and 6000 K, and then cooled to 4000 K. These simulations were performed with the x and y dimensions held constant and a stress of 5 GPa applied parallel to the z axis. At 3000 K, the crystals were released to allow for interchange of species between the crystals and the IGF, and the systems were then quenched to 2000 K under a stress of 3 GPa applied parallel to the z axis. Next, the systems were cooled to 1000 K, and then to 300 K, under conditions of a constant pressure of 0.1 MPa and constant number and temperature (NpT). A simulation time step of 1×10^{-15} s was used throughout the simulations.

TABLE I. Parameters for modified BMH pair potential function.

Atom pair	A_{ij} (fJ)	β_{ij} (pm)	ρ_{ij} (pm)
O–O	0.0725	234	29
Si–Si	0.1877	230	29
Ca–Ca	0.7000	230	29
N–N	0.07241	261	29
Si–Ca	0.2215	230	29
Si–N	0.7800	241.3	25.89
N–Ca	0.8600	234	29
Si–O	0.2962	234	29
N–O	0.1350	230	29
Ca–O	0.5700	234	29

BMH, Born–Mayer–Huggins.

TABLE II. Parameters for 3-Body Potential Function.

Atom triplet	λ_{ij} (fJ)	γ_{ij} (pm)	r_{ij}^0 (pm)	θ_{jik}^0 (deg)
Si/Ca–O–Si/Ca	0.001	200	260	109.5
Si–N–Si	0.035	260	280	120
O/N–Si–O/N	0.024	280	300	109.5

III. RESULTS AND DISCUSSION

Figure 1 shows 10 Å slices at the center of the initial and final configuration in which two prism Si_3N_4 planes are in contact with the IGF. The large, dark spheres in Fig. 1 represent Si ions that are originally in the IGF; the large, gray spheres represent Ca ions; the large, lighter shaded spheres represent O ions; the small, dark spheres represent Si ions that are originally in the crystal; the small lighter shaded spheres represent N ions. Similarly, Fig. 2 shows 10 Å slices at the center of the initial and final configuration in which the IGF is in contact with two basal Si_3N_4 planes. Despite the complete spatial disorder of the silicate atoms at the beginning of the simulations, the final configurations of the IGF are

TABLE III. Heat and quench process.

Quench temperature	Conditions	Duration
10,000K	NVE, crystal frozen	10 ps
8000K	x, y constant, P_z = 5 GPa	10 ps
6000K	As above	10 ps
4000K	As above	40 ps
3000K	x, y constant, P_z = 3 GPA, crystal de-frozen	40 ps
2000K	NpT, p = 0.1 MPa	10 ps
1000K	As above	10 ps
300K	As above	20 ps

NVE, constant number, volume, energy; NpT, constant number, pressure, temperature.

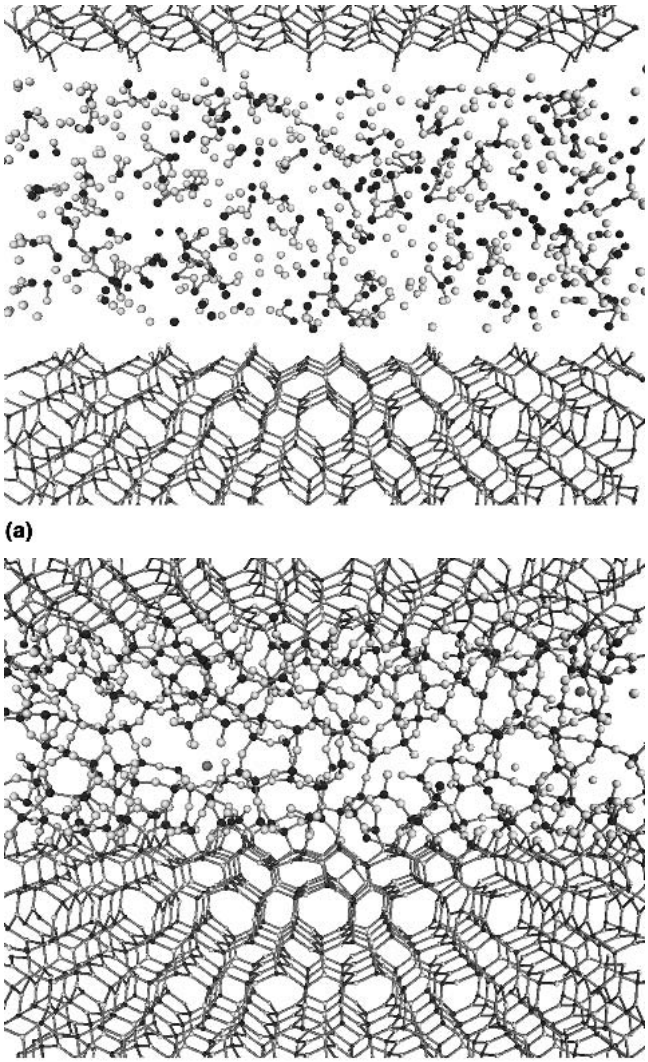

FIG. 1. Ten angstrom (10 Å) slices at the center of the (a) initial and (b) final configurations in which two prism Si_3N_4 planes are in contact with the IGF. The large, dark spheres represent Si ions that are originally in the IGF; the large, gray spheres represent Ca ions; the large, lighter shaded spheres represent O ions; the small, dark spheres represent Si ions that are originally in the crystal; the small lighter shaded spheres represent N ions.

well-ordered in the interface region in both the prism and basal cases. For the sake of simplicity, we use Si-c to represent Si ions that originally come from the Si_3N_4 crystal and Si-g as Si ions that originally come from the random mixtures of atoms in the IGF.

Figure 3 shows the atom number density of all species along z axis in the final configuration, with two prism and two basal crystal Si_3N_4 planes. In both the prism and basal cases, the atom number densities of both Si-g and O reach their minimum peak values near the center of the IGF while having the maximum peak values at the interface with the crystals. In addition, there is ordering at the interfaces and oscillations in the peak heights. For the prism case, the spacing between the first O peak in the IGF and the last peak in crystal Si_3N_4 is approximately 2.0 Å, and in the interior of the IGF, the spacing between O peaks is approximately 2.3 Å [Fig. 3(a)]. In the basal case, the spacing between the first O peak in the IGF and the last peak in crystal Si_3N_4 is approximately 1.0 Å, and the spacing between O peaks is approximately 2.3 Å in the interior of the IGF [Fig. 3(b)]. The thickness of the IGF in both the prism and basal cases is approximately 15 Å, although this thickness is dictated by the number of ions in the IGF. A small number of N-c ions move into the IGF near the interface, and more of this occurs with the prism case than the basal case, indicating the greater stability of the basal plane than the prism plane. Meanwhile, O ions also moved into the N sites in the crystal. Both events, N ions into IGF and O ions into crystal

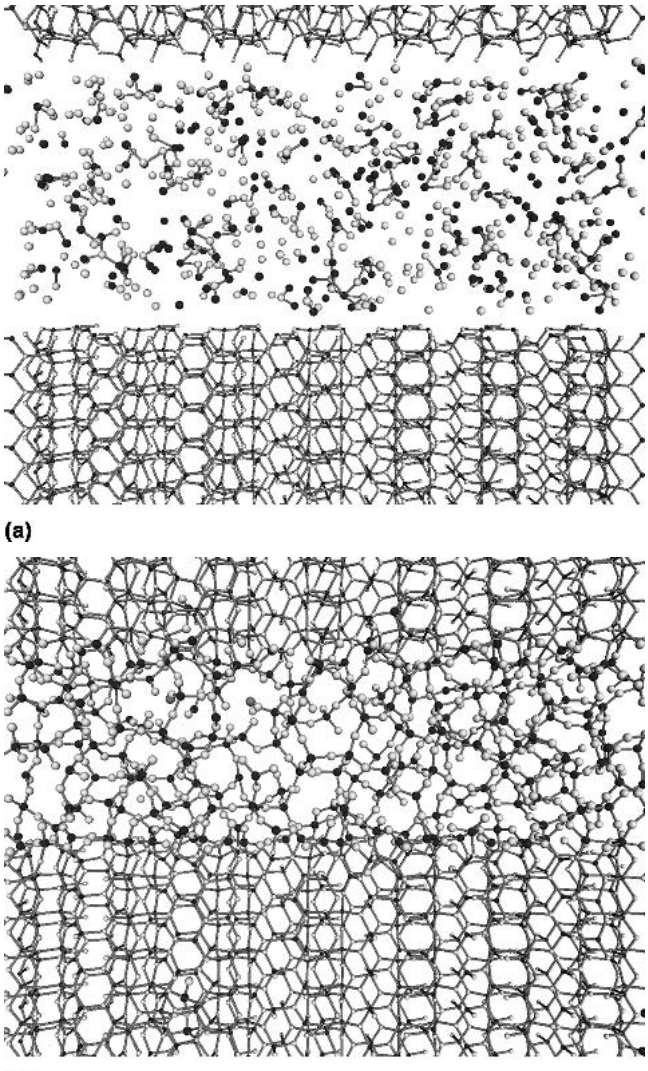

FIG. 2. Ten angstrom (10 Å) slices at the center of the (a) initial and (b) final configurations in which two basal Si_3N_4 planes are in contact with the IGF. Size and shade schemes are the same as in Fig. 1.

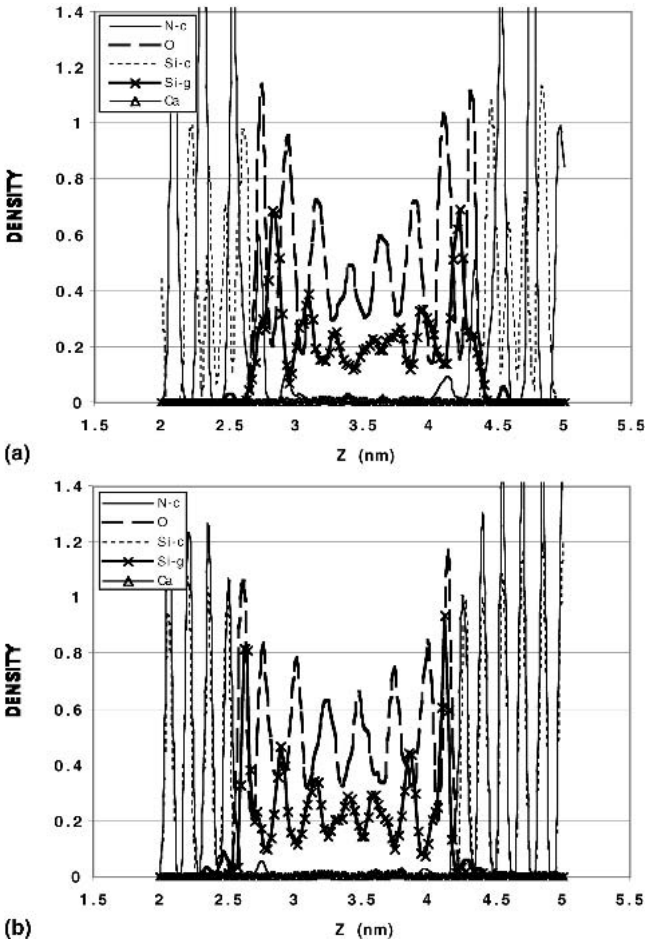

FIG. 3. The atom number density of all species along z axis in the final configurations with (a) two prism crystal Si_3N_4 planes and (b) two basal crystal Si_3N_4 planes.

surface, indicate the formation of a Si–O–N interface. In addition, Ca ions do not segregate to the IGF–crystal interface, contrary to the case of the calcium silicate intergranular films between basal planes in alumina, where Ca additives segregated preferentially into the ordered Al_2O_3/SiO_2 regions.[20]

Figure 4 shows the coordination number of O ions across the IGF in the final configuration, between two prism and two basal crystal Si_3N_4 planes. While the majority of O ions are 2-coordinated in both the prism and basal cases, a small portion of O ions are 1-coordinated, consistent with the presence of Ca ions located in the interior of the IGF. An even smaller portion of O ions are 3-coordinated, located at the interface of the IGF. However, there is a larger portion of 3-coordinated O ions in the basal case than in the prism case, indicating that there are more defects in the basal case at the interface of the IGF.

From Fig. 3, the highest number density of O ions in both the prism and basal cases is found at the interface, where the IGF is connected with the Si_3N_4 crystal. So it is important to investigate how the O ions at the interface are bonded with neighbor Si ions. Si ions on crystal lattice sites are denoted as Si-surf, regardless of whether the Si came from Si-c or adsorbed Si-g. Si-g ions that are not adsorbed onto the crystal are denoted as Si-igf. Figure 5 shows the coordination numbers of the O ions adsorbed at the interface in the final configuration. Thus, these O have at least one bond to the Si on the crystal surface lattice, labeled Si-surf. The O coordination number is delineated as a function of the type of Si, m and n, to which the O ions are attached, where m is the coordination number of O with Si-surf ions and n is the coordination number with Si-igf ions. In Fig. 5, the white histograms are for O adsorbed onto the prism planes, while the black histograms are for O adsorbed onto the basal planes. While the majority of the O ions adsorbed at the surfaces of either crystal orientation are twofold coordinated, there is an important difference in the type of coordination (m, n) that occurs at each surface.

For the prism case, the majority of O ions at the interface have the coordination numbers (1, 1); in other words, they form bonds with one Si-surf ion and one

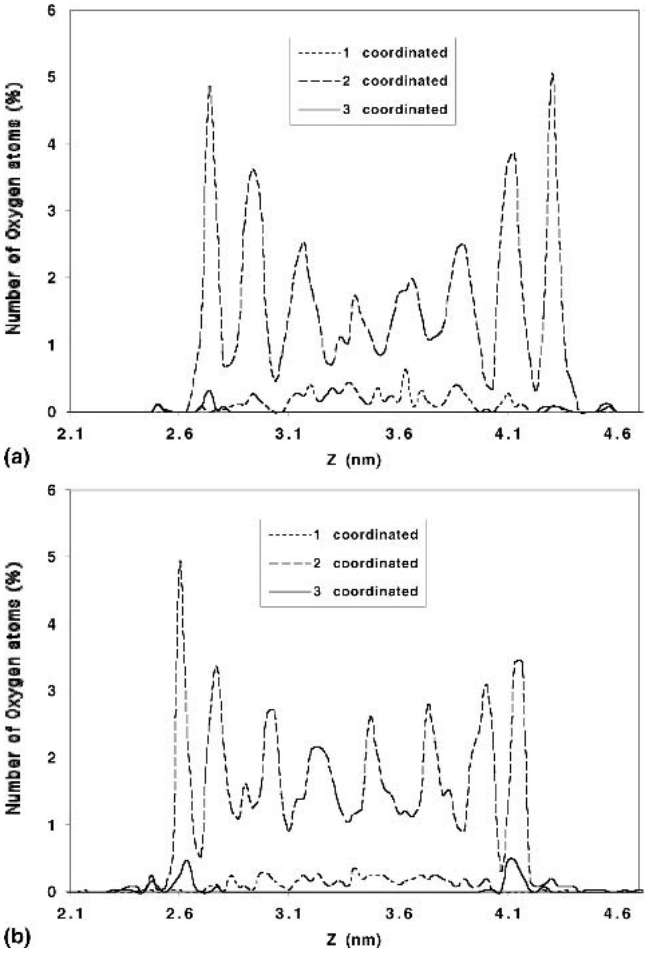

FIG. 4. The coordination number of O ions across the IGF in the final configurations with (a) two prism crystal Si_3N_4 planes and (b) two basal crystal Si_3N_4 planes.

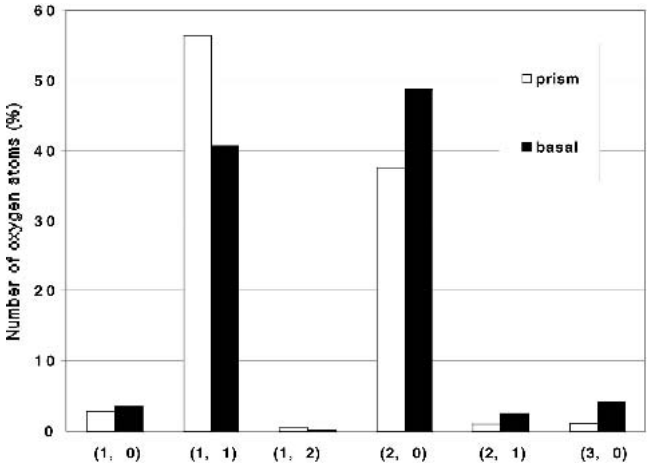

FIG. 5. The coordination numbers (m, n) of the O ions at the interface in the final configuration, with two prism (white histograms) and two basal (black histograms) crystal Si_3N_4 planes, respectively, where m is the coordination number with neighbor Si-surf ions and n is the coordination number with neighbor Si-igf ions.

Si-igf ion. The second largest portion of O ions at the interface have the coordination numbers (2, 0); that is, they form bonds with two Si-surf ions. For the basal case, however, the largest portion of O ions at the interface has the coordination numbers (2, 0). The next largest portion of O ions at the basal interfaces has the coordination numbers (1, 1). While there are only a few 3-coordinated (3CN) O at either interface, there are more associated with the basal plane orientation, especially those with three bonds to the Si-surf. These latter O are ions that have adsorbed onto the N lattice sites of the crystal, creating the 3CN of these O. The nonbridging O (NBO) that exist at the interface are nearly equivalent on the two crystal orientations. As discussed previously,[23] NBO adsorbed at the interface would have important implications regarding the connectivity between the two crystal surfaces via the IGF. Increasing the concentration of such NBO that are localized along a 2d plane parallel to the crystal–IGF interface would have a more dramatic effect on weakening the connectivity between the grains (via the IGF), thus increasing the ease of sliding or enhancing grain separation. Here, the small concentrations of NBO are similar to the data observed in the earlier work using a pure silica IGF between two basal planes.[23] However, while the concentration of NBO are similar at these low Ca concentration IGFs, the above-mentioned differences in the 2-coordinated O at the prism and basal planes have other implications.

Considering the 2- and 3-coordinated O at the interface, the bonding characteristics of the O ions at the interface with neighbor Si-surf and Si-igf ions are different in the prism and basal cases. Previous simulations of silicate IGFs between basal planes showed an important effect on NBO (1, 0) formation caused by increasing CaO concentration in the IGF at constant film thickness or decreasing the IGF thickness at constant composition.[23] Those simulations showed that the formation of NBO (1, 0) at the interface occurred at the preferential expense (loss) of 2-coordinated O in the (1, 1) configuration at the interface rather than the (2, 0) configuration. Based on this data and the larger concentration of (1, 1) O at the interfaces with the prism planes may indicate that the prism surfaces would be more prone to formation of these localized (1, 0) NBO. Such an increased formation of localized NBO would create a greater weakening of the system of grains connected via prism planes.

From Figs. 1 and 2, the atomistic structure of the IGF is found to be different at the interface than in the interior of the IGF. In addition, it is expected that the difference in bonding structure of the different terminations, prism versus basal, would affect structure at the interfaces. In the prism crystal Si_3N_4 surface, the coordinatively undersaturated (CUS) Si and N ions are located in different planes, each of them missing one bond. In the basal crystal Si_3N_4 surface, however, the CUS Si and N ions are located in the same plane, each of them missing two bonds. Analysis of the detailed bonding at these interfaces shows the effects of these differences.

The partial pair distribution function (PDF) of Si versus O at the interface and in the interior of the IGF was calculated by using Si as central ions in the final configuration with two prism and two basal crystal Si_3N_4 planes, as shown in Fig. 6. In both cases, the intensity of the first peak in the Si–O PDF is smaller for that associated with central Si located at the interface versus central Si still within the IGF, indicating the lower coordination of Si at the interface to O caused by the presence of competing Si–N bonds at the interface. In the prism case, Fig. 6(a), the first peak of the PDF for interface Si and O ions is located at 1.64 Å whereas the first peak for interior Si and O ions is found at 1.62 Å. For the basal case, Fig. 6(b), the first peak of the Si–O PDF is located at 1.62 Å, both at the interface and in the interior of the IGF. This indicates that the Si–O bond length over the whole IGF (interface and interior) has a range from 1.62 Å to 1.64 Å, consistent with recent experimental findings,[24] in which the Si–O bond length was found to be 1.64 ± 0.04 Å. Figure 7 is a close-up view of the first peak of the Si–O PDFs in Fig. 6. Clearly, the first peak of PDF for interface Si and O ions in the prism case shifts to the right of the basal case whereas only a slight shift is observed for interior Si and O ions in the prism case relative to the basal case.

However, the simulations provide more specific data regarding the locations of different Si–O bond lengths, as well as an apparent difference between Si–O bonds between basal surfaces versus those between prism surfaces. The simulations indicate that between the prism surfaces, the Si–O bonds are more strained (elongated) at

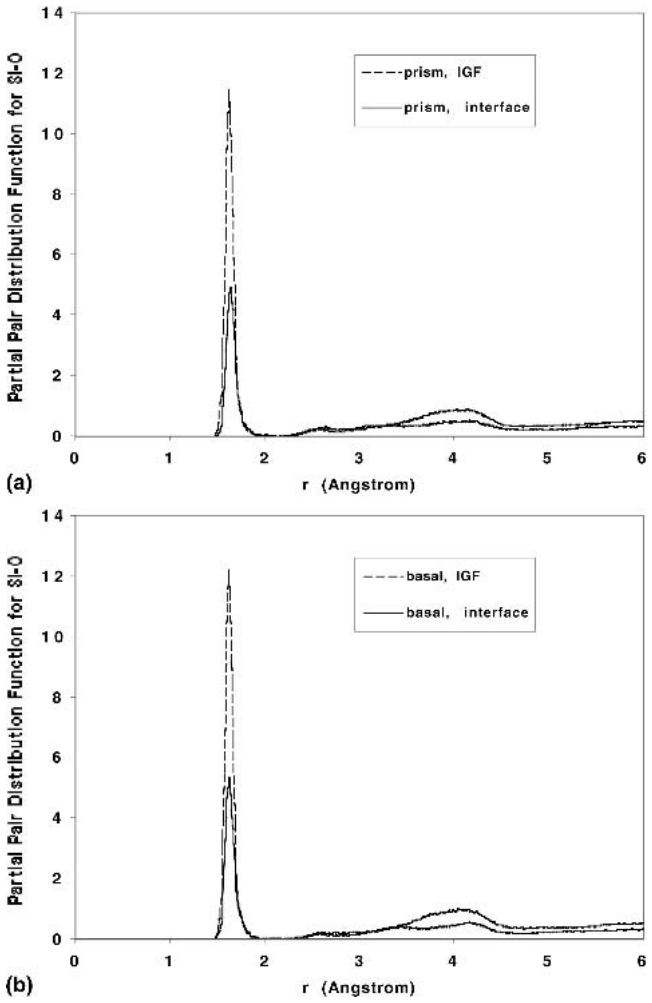

FIG. 6. The partial PDF of Si versus O at the interface and in the interior of the IGF in the final configurations with (a) two prism crystal Si_3N_4 planes and (b) two basal crystal Si_3N_4 planes.

the interface than those in the interior of the IGF. In fact, the peak maximum in the Si–O PDF at the interior between both the basal and prism planes is the same as that found in bulk silica glass (1.62 Å). However, distortions appear to be greater for Si–O bonds between the prism surfaces at the interface. Because there is a larger portion of 3-coordinated O ions in the basal case than in the prism case, one tends to expect that the Si–O bond length be larger in the basal case due to the longer bond lengths associated with those 3CN O. However, we observed the opposite: the Si–O bond length is larger between the prism surfaces, especially at the interface. To resolve this discrepancy, we calculated the PDF of O versus Si by using O as central ions at the interface, in the interior of the IGF, and exclusively the 3CN O, for both the prism and basal cases, as shown in Fig. 8. The central position of the peaks for the 3CN O is roughly located at 1.73 Å, which is approximately 0.1 Å larger than the central position of all other peaks. Similar to the Si–O PDFs calculated by using Si as central ions, as shown in Fig. 7, the

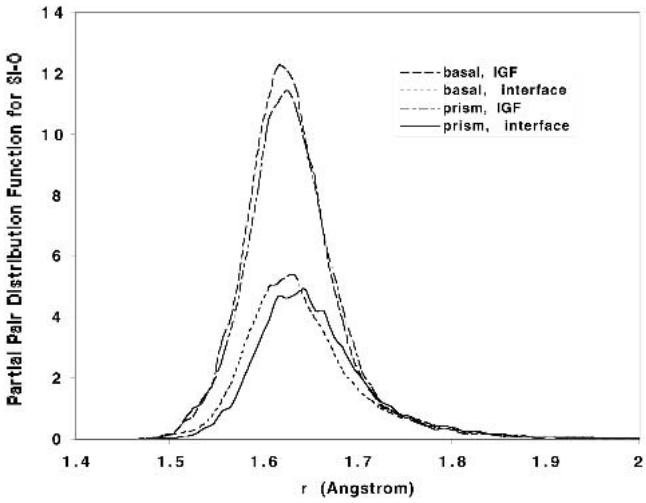

FIG. 7. A close-up view of the first peak of the Si–O PDFs in Fig. 6.

first peak of PDF for interface Si and O ions in the prism case shifts to the right of the basal case. Although the 3CN O cause the intensity of the PDFs for interface Si and O ions to be slightly higher than those for interior IGF ions at approximately 1.73 Å, they do not cause the shift of the first peak for interface Si and O ions in the prism case. Furthermore, the number of 3CN O is only about one-fifth that of the 2CN O at the interface, making their contribution to the shift even less.

Another important feature observed in the simulations is the increase in intensity in the Si–O PDF between 2.4 and 3 Å. In bulk silicate glasses, the intensity in this region is close to zero. The increase shown in these simulations is apparently due to the ordering induced by the interfaces. Evaluation of this behavior via an experimental PDF would be valuable.

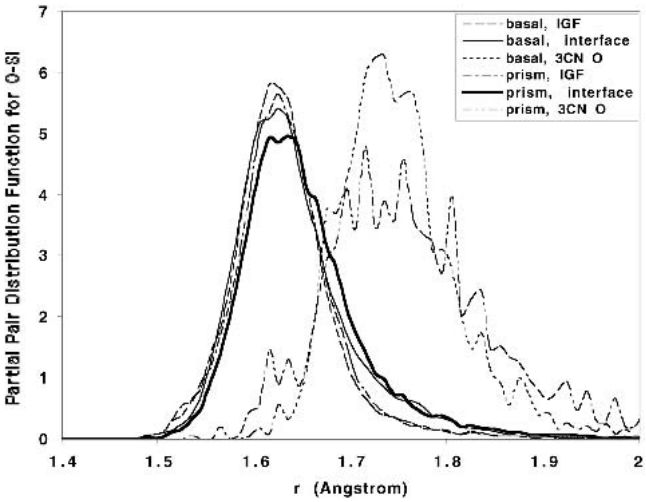

FIG. 8. A close-up view of the first peak of the PDFs of O versus Si at the interface, in the interior of the IGF, and exclusively the 3CN O, for both the prism and basal cases.

IV. CONCLUSIONS

Molecular dynamics simulations of IGFs containing SiO_2 and CaO in contact with two prism $(10\bar{1}0)$ and two basal (0001) planes of Si_3N_4 was performed using a multibody interatomic potential. Samples with the same composition and number of atoms but different crystal planes (i.e., the prism and basal planes) of Si_3N_4 were studied. The final configuration of the IGF in both the prism and basal cases showed ordering in the interface region induced by the crystal surfaces. The thickness of the IGF in both cases is approximately 15 Å. It is found that a small number of N ions from the crystals moved into the IGF near the interface, and O ions also moved into the N sites in the crystal, indicating the formation of a Si–O–N interface. In addition, Ca ions do not segregate to the IGF–crystal interface. While the majority of O ions are 2-coordinated in both the prism and basal cases, a small portion of O ions are 1-coordinated, consistent with the presence of Ca ions located in the interior of the IGF. An even smaller portion of O ions are 3-coordinated, located at the interface between the IGF and the crystals. For the prism case, the majority of O ions at the interface form bonds with one Si-surf ion and one Si-igf ion. The second largest portion of O ions at the interface form bonds with two Si-surf ions. For the basal case, however, the largest portion of O ions at the interface form bonds with two Si-surf ions. The next largest portion of O ions at the basal interfaces form bonds with one Si-surf ion and one Si-igf ion. At either interface, there are only a few 3-coordinated O, which are more associated with the basal plane orientation, especially those with 3 bonds to the Si-surf. Such O ions have adsorbed onto the N lattice sites of the crystal. Finally, the Si–O bond length of the IGF has a range from 1.62 Å to 1.64 Å, consistent with recent experimental findings. The simulations provide more specific data regarding the locations of different Si–O bond lengths as well as an apparent difference between Si–O bonds between basal surfaces versus those between prism surfaces.

ACKNOWLEDGMENTS

The authors acknowledge support from United States Department of Energy OBES Materials Sciences DE-FG02-00ER45823 and partial support for X.S. from the National Science Foundation Award DMR-0010062.

REFERENCES

1. D.R. Clarke and G. Thomas, J. Am. Ceram. Soc. **60,** 491 (1977).
2. D.R. Clarke and G. Thomas, J. Am. Ceram. Soc. **61,** 114 (1978).
3. D.R. Clarke and G. Thomas, Ultramicroscopy **4,** 33 (1979).
4. R. Raj, J. Geophys. Res. B **87,** 4731 (1982).
5. R.L. Tsai and R. Raj, J. Am. Ceram. Soc. **63,** 513 (1980).
6. F.F. Lange, Am. Ceram. Soc. Bull. **62,** 1368 (1983).
7. H-J. Kleebe, M.J. Hoffmann, and M. Rühle, Z. Metallkd **83,** 610 (1992).
8. M.K. Cinibulk, H-J. Kleebe, and M. Rühle, J. Am. Ceram. Soc. **76,** 426 (1993).
9. H-J. Kleebe, M.K. Cinibulk, R.M. Cannon, and M. Rühle, J. Am. Ceram. Soc. **76,** 1969 (1993).
10. D. Clarke, J. Am. Ceram. Soc. **70,** 15 (1987).
11. D.R. Clarke, T.M. Shaw, A.P. Philipse, and R.G. Horn, J. Am. Ceram. Soc. **76,** 1201 (1993).
12. I. Tanaka, H.J. Kleebe, M.K. Cinibulk, J. Bruley, D.R. Clarke, and M. Rühle, J. Am. Ceram. Soc. **77,** 911 (1994).
13. B.F. Feuston and S.H. Garofalini, J. Chem. Phys. **91,** 564 (1989).
14. S.H. Garofalini, J. Non-Cryst. Solids **120,** 1 (1990).
15. D.M. Zirl and S.H. Garofalini, J. Am. Ceram. Soc. **73,** 2848 (1990).
16. S.H. Garofalini, in *Reviews in Mineralogy and Geochemistry: Molecular Modeling Theory: Applications to the Geosciences*, **42,** edited by R. Cygan and J. Kubicki (Mineralogical Society of America, Washington, DC, 2001), p. 131.
17. L. Cormier, D. Ghaleb, J-M. Delaye, and G. Calas, Phys. Rev. B **61,** 14495 (2000).
18. J-M. Delaye, V. Louis-Achille, and D. Ghaleb, J. Non-Cryst. Solids **210,** 232 (1997).
19. K. Yamahara and K. Okazaki, Fluid Phase Equilib. **144,** 449 (1997).
20. S. Blonski and S.H. Garofalini, J. Am. Ceram. Soc. **80,** 1997 (1997).
21. M. Garcia, E. Webb, and S.H. Garofalini, J. Electrochem. Soc. **145,** 2155 (1998).
22. M. Garcia and S.H. Garofalini, J. Electrochem. Soc. **146,** 840 (1999).
23. S.H. Garofalini and W. Luo, J. Am. Ceram. Soc. **86,** 1741 (2003).
24. W. McBride and D.J.H. Cockayne, J. Non-Cryst. Solids **318,** 233 (2003).